Carcinogenesis, 2020, Vol. 41, No. 3, 313–325

doi:10.1093/carcin/bgz172
Advance Access Publication October 17, 2019
Original Article

ORIGINAL ARTICLE

TIMP-2 suppresses tumor growth and metastasis in murine model of triple-negative breast cancer

David Peeney[1,†], Sandra M. Jensen[1,†], Nadia P. Castro[2,†], Sarvesh Kumar[1], Silvia Noonan[1], Chenchen Handler[1], Alex Kuznetsov[1], Joanna Shih[3], Andy D. Tran[4], David S. Salomon[2] and William G. Stetler-Stevenson[1,*]

[1]Extracellular Matrix Pathology Section, Laboratory of Pathology, Center for Cancer Research, National Cancer Institute, Bethesda, MD 20892, USA, [2]Tumor Growth Factor Section, Mouse Cancer Genetics Program, National Cancer Institute, Frederick, MD 21702, USA, [3]Biostatistics Branch, National Cancer Institute, Rockville, MD 20850, USA and [4]Confocal Core Facility, National Cancer Institute, Bethesda, MD 20892, USA

*To whom correspondence should be addressed. Tel: +1 240 760 6105; Fax: +1 240 541 4539; Email: sstevenw@mail.nih.gov
†These authors contributed equally to this work.

Abstract

Metastasis is the primary cause of treatment failures and mortality in most cancers. Triple-negative breast cancer (TNBC) is refractory to treatment and rapidly progresses to disseminated disease. We utilized an orthotopic mouse model that molecularly and phenotypically resembles human TNBC to study the effects of exogenous, daily tissue inhibitor of metalloproteinase-2 (TIMP-2) treatment on tumor growth and metastasis. Our results demonstrated that TIMP-2 treatment maximally suppressed primary tumor growth by ~36–50% and pulmonary metastasis by >92%. Immunostaining assays confirmed disruption of the epithelial to mesenchymal transition (EMT) and promotion of vascular integrity in primary tumor tissues. Immunostaining and RNA sequencing analysis of lung tissue lysates from tumor-bearing mice identified significant changes associated with metastatic colony formation. Specifically, TIMP-2 treatment disrupts periostin localization and critical cell-signaling pathways, including canonical Wnt signaling involved in EMT, as well as PI3K signaling, which modulates proliferative and metastatic behavior through p27 phosphorylation/localization. In conclusion, our study provides evidence in support of a role for TIMP-2 in suppression of triple-negative breast cancer growth and metastasis through modulation of the epithelial to mesenchymal transition, vascular normalization, and signaling pathways associated with metastatic outgrowth. Our findings suggest that TIMP-2, a constituent of the extracellular matrix in normal tissues, may have both direct and systemic antitumor and metastasis suppressor effects, suggesting potential utility in the clinical management of breast cancer progression.

Introduction

The major cause of cancer-related deaths is dissemination of 1° tumor cells and establishment of therapeutically resistant lesions at distant sites. Metastasis formation has long been viewed as a result of systemic changes at specific secondary sites that are the results of 1° tumor influences. This is the original 'seed and soil' hypothesis of Paget that was further refined by Fidler in defining the role of 'organotropism' during the metastatic cascade (1,2). The formation, survival, and expansion of metastatic foci are influenced by multiple interactions within the local tumor microenvironment [TME], including development of a vasculature, alteration in the composition and structure of the stroma, as well as conditioning of immune cell populations, each providing a framework for potential targeted therapies (3–5). These changes are the result of tumor cell reprogramming of stromal cells in normal tissues to generate a local environment that promotes successful metastatic outgrowth, known as the

Received: 16 May 2019; **Revised:** 12 September 2019; **Accepted:** 11 October 2019
Published by Oxford University Press 2019.

Abbreviations

ECM	extracellular matrix
EM	expectation-maximization
EMEM	Eagle's minimal essential media
EMT	epithelial-to-mesenchymal transition
FBS	fetal bovine serum
GSA	gene specific analysis
HBSS	Hanks Balanced Salt Solution
MMPs	matrix metalloproteases
PCA	Principle component analysis
TIMPs	tissue inhibitors of metalloproteinases
TNBCs	Triple-negative breast cancers

premetastatic/metastatic niche (PMN) (6,7). Recent studies have focused on identifying specific tumor-induced changes in the extracellular matrix (ECM) and immune cell modulation of the TME at these secondary sites of tumor formation.

Early studies demonstrated tumor cell invasion requiring proteolytic degradation of the ECM as a prerequisite for metastasis formation and implicated matrix metalloproteases [MMPs], a large family of metzincin proteinases (8,9). The proteolytic activity of the MMPs is tightly regulated by natural inhibitors known as the tissue inhibitors of metalloproteinases (TIMPs), a family of four proteins that plays a role in regulating ECM remodeling and cellular functions in both normal and disease states (10–12). TIMPs suppress tumor cell migration and invasion *in vitro*, which led to the development of synthetic, nonselective MMP inhibitors. However, failure of the synthetic compounds in early patient trials curtailed much of the initial enthusiasm for clinical application of all MMP inhibitors (13). TIMP-2 is a plasma protein that is widely expressed in the stromal compartment of normal tissues, and in the context of cancer has been shown to possess novel functions, some MMP-independent, including inhibition of tumor growth and angiogenesis, reducing vascular permeability, suppression of tumor cell migration and invasion, as well as inhibition of the epithelial-to-mesenchymal transition [EMT] (14–18). These findings suggest potential clinical utility of TIMP-2 in the development of novel cancer therapies.

Triple-negative breast cancers [TNBCs] are a diverse group of biologically aggressive tumors lacking estrogen and progesterone receptors (ER and PR, respectively), as well as the human epidermal growth factor receptor 2 (HER2). TNBC therapies remain limited and ineffective due to the lack of specific targets and rapid progression (19). Therefore, continued development of novel therapies remains imperative and will require systemic therapies for successful treatment of metastatic disease in TNBC patients.

In the current study, we examine the impact of TIMP-2 administration, both *in vitro* and *in vivo* on TNBC growth and metastasis. Utilizing an orthotopic mouse model that was extensively characterized to demonstrate phenotypic and molecular resemblance to the human disease (20), we show that TIMP-2 treatment TIMP-2 treatment restrains 1° TNBC tumor growth, suppresses EMT and pulmonary metastasis, as well as enhances vascular normalization *in vivo*. In addition, we examine pulmonary metastasis for p27 and periostin [POSTN] expression, as well as adjacent uninvolved lung tissues by RNA-sequencing analysis for changes in gene expression associated with the metastatic colonization. These results are the first demonstration that TIMP-2 treatment enhanced tumor cell nuclear localization of p27, reduced POSTN expression, and suppressed cell signaling pathways frequently activated in formation of the breast cancer metastasis. Together, these data provide evidence for the potential utility of TIMP-2 in the clinical management of TNBC progression and metastasis.

Materials and methods

Cell line authentication

The murine JygMC(A) cell line was originally isolated from a spontaneous, metastatic mammary carcinoma arising in a Chinese feral mouse (*Mus musculus* Sub-Jyg), obtained by our laboratories from the University of Tokyo, Japan (gift of Dr Shogo Ehata, December 2011) under standard NIH Materials Transfer Agreement. The JygMC(A) cell line was expanded through passage (<3; DMEM + 10% FBS) upon receipt to generate frozen stocks (–80°C) of the original cells. JygMC(A) cells were extensively tested, characterized, and authenticated in our laboratories by whole genome transcriptome microarray analysis utilizing murine specific platforms (STR analysis is not performed on murine cell lines due to limited data bases), to definitively demonstrate that JygMC(A) cells are murine mammary carcinoma with a triple-negative phenotype, as we have previously reported (20,21). JygMC(A) cells were certified pathogen free (Molecular Testing of Biologic Material; MTBM #1046-1 January 2012) and suitable for use in *nu/nu* (nude) mouse studies by the Animal Health Diagnostic Laboratory, NCI-Frederick. In the current study, frozen stocks of the original JygMC(A) cultures and reauthenticated using methods described above. The 4T1 cell line was obtained from American Type Culture Collection Repository and certified pathogen free (MTBM testing).

Preparation of TIMP-2 for in vivo use

Recombinant TIMP-2 (TIMP-2) with 6X His-epitope tag was expressed, purified, and tested negative for Endotoxin in the MTBM assay (Animal Health Diagnostic Laboratory, NCI-Frederick) (22). TIMP-2 preps showed >98% purity. Protein concentration was determined by A_{280}, bicinchoninic acid (BCA) assay, and sandwich ELISA assays. Lyophilized TIMP-2 powder was reconstituted in Hanks Balanced Salt Solution (HBSS), sterile filtered (0.22 μm), and stored at –80°C until use.

In vitro assay of TNBC cell growth, invasion, and gene expression

For the analysis of tumor cell growth and invasion, we assessed spheroid outgrowth into 3D matrix (Cultrex basement membrane extract, Trevigen). Briefly, JygMC(A) or 4T1 cells were seeded at 2500 cells per well of a 96-well ultralow attachment, round bottomed plate in Eagle's minimal essential media (EMEM) containing 10% fetal bovine serum (FBS) and allowed to form spheroids over 6 days. Spheroids were placed on top of a bed 50 μl polymerized 3D matrix and covered with 50 μl EMEM 2% FBS supplemented with 0.4 mg/ml 3D matrix. Additionally, 4T1 cells were supplemented with 10 ng/ml TGFβ to maintain spheroid integrity. Spheroids were imaged at ×4 magnification on day 0 and day 4 (n = 8 individual wells). Increase in spheroid size was quantified using the Adobe Photoshop measure function to quantify individual pixels (see Supplementary Figure 1A, available at *Carcinogenesis* Online).

For the *in vitro* assessment of protein expression following TIMP-2 treatment, JygMC(A) or 4T1 cells were seeded in 96-well plates at 2500 cells per well, incubated for 24 h, and serum starved in EMEM overnight. Serum-starved cells were then cultured in EMEM 0.1% FBS for 72 h with/without 1 μg/ml TIMP-2. Cell lysates were harvested using 10 μl/well radioimmunoprecipitation (RIPA) buffer containing 1% protease/phosphatase inhibitor cocktail and pooled for immunoblot analysis.

TIMP-2 treatment effect on TNBC growth and metastasis

The *in vivo* effects of TIMP-2 on TNBC growth and metastasis were studied using the orthotopic JygMC(A) model that develops spontaneous lung metastases (20). Briefly, athymic, female *nu/nu* (nude) mice (6–9 weeks of age) were obtained from NCI at Frederick, Maryland, and procedures were approved by the NCI Animal Care and Use Committee (AAALAC accredited institution; Protocols #1-067 and LP-003). JygMC(A) cells (20 μl of 5 × 10^4 cells/mouse) were injected into fourth inguinal mammary fat pads on day

zero. On day 10 or 11 mice were randomized based on tumor size and daily i.*p.* TIMP-2 or vehicle control (HBSS) injections were initiated. Primary (1°) tumor size was assessed using tri-weekly caliper measurement to calculate tumor volumes (Vol.) plotted as mean tumor volume (mm^3 ± SEM) for each group, as previously reported (20). Growth inhibition of 1° tumor growth was calculated using [growth inhibition = $1–(Vol._{TIMP-2}/Vol._{control}) \times 100$], where $Vol._{TIMP-2}$ and $Vol._{control}$ are the mean tumor volumes for each experimental group observed. Growth inhibition values were calculated on day 31 for Exp #1–3. In later experiments, surgical resections of the primary tumors were performed on day 32 as indicated and TIMP-2 treatment continued for an additional 7 days, until day 39 (see Figure 2A). At the termination of the experiment on day 52, mice were euthanized, and the lungs were excised *en bloc* for assessment of metastasis.

Immunostaining

Immunohistochemistry and immunofluorescence studies

Immunohistochemistry (IHC) and immunofluorescence (IF) were performed on formalin-fixed, paraffin-embedded tissue sections (FFPE) using standard laboratory practices for tissue processing, embedding, section, and staining. Primary antibodies are listed in Supplementary Table 1, available at *Carcinogenesis* Online. Immunohistochemical results were assessed using an index (SI) modified from the Allred scoring system (23).

Image analysis

ImageJ/FIJI software was used to quantify type IV collagen [Col-IV] staining intensity of confocal images. Vessels were segmented by outlining $CD31^+$ cells, then dilated by five microns to create region of interest. The mean fluorescence intensity of Col-IV within this border region of interest was quantified, and *P*-values were calculated using a two-tailed Mann–Whitney *U*-test. Colocalization of p27 and DAPI-labeled nuclei was calculated using Zen Black software (Zeiss) using intensity thresholds determined from single-stained controls. The Mander's coefficient was used to denote the overlap of p27 with DAPI-labeled nuclei. POSTN staining was assessed by generating geometric statistics for both area and major/minor axis ratio using the Kolmogorov–Smirnov two-sample test (Peacock Test) and quantified by the Mann–Whitney *U* two-tailed test.

Vascular permeability assay

To examine vascular permeability in primary TNBC tumors, mice (n = 3/experimental group) were injected intravenously with rhodamine B-conjugated dextran (70 kDa, Thermo Scientific D1841) using 0.1 mg/g body weight, euthanized three hours post injection, resected 1° tumors were fixed in 4% paraformaldehyde overnight at 4°C, before sinking in 15–30% sucrose gradient, then frozen in OCT and stored at –80°C prior to sectioning, as described (24). Confocal imaging (LSM710, Zeiss) of extravasated rhodamine B-conjugated dextran was quantified using Image J Software.

RNA sequencing

To examine changes in gene expression associated with formation of pulmonary metastasis, we performed RNA sequencing analysis on nontumor containing, whole lung tissues (referred to as uninvolved lung) obtained from 5 tumor bearing mice per experimental group. Snap frozen lungs were thawed overnight in RNA later (ThermoFisher) at 4°C, and tumor-free lung tissue samples were obtained using a dissecting microscope. Dissected, tumor-free tissues from each lung sample were evenly divided for protein and RNA extraction. RNA extraction was performed in Trizol using gentleMACS dissociator and M tubes (Miltenyi Biotech) with the manufacturers optimized settings for fresh tissue. RNA samples were cleaned using a RNeasy mini kit (Qiagen), and RNA quality was determined using TapeStation (Agilent) and Bioanalyzer 2100 (Agilent). RIN values (4.9–7.2) indicated all samples were appropriate for RNA sequencing analysis that was performed using a HiSeq 4000 (Illumina) and TruSeq Stranded Total RNA Kit (Illumina) with paired-end sequencing and a 60 to 100 million pass filter read with a base call quality of >92% bases with Q30 or higher. Data normalization and analysis was performed using Partek Flow software. Read contaminants and low-quality reads (Phred score <20) were removed using Bowtie 2. Trimmed reads were aligned to the mouse (mm10) genome using STAR and annotated to RefSeq transcripts using Partek's expectation-maximization (EM) algorithm. Principle component analysis (PCA) of normalized data was performed using Partek Genomics Suite®. Pearson's correlation cluster heatmaps were generated with R statistical programming using the gplots package. Differential gene expression (GSA) was performed with a fold change and false discovery rate cutoffs of 1.5 and 0.5, respectively. Significant gene changes highlighted by GSA were imported into Ingenuity Pathway Analysis for gene set enrichment analysis.

Immunoblotting analysis

Total protein homogenates were prepared from tissue culture cell lysates or tumor-free lung tissues in RIPA buffer containing 1% protease and phosphatase inhibitors. Total protein was determined by BCA Protein Assay (Thermo Scientific, USA), resolved by sodium dodecyl sulfate–polyacrylamide gel electrophoresis and electrophoretically transferred onto nitrocellulose membranes. Immunoblotting was performed using standard methods with β-actin or glyceraldehyde 3-phosphate dehydrogenase as loading controls (SuperSignal West Pico Plus, ThermoFisher Scientific). Protein bands were visualized using the ChemiDoc™ XRS+ imaging system and quantified by Image Lab Version 5.2.1 Software (BIO-RAD, USA).

Results

Initial in vitro experiments

Utilizing the *in vitro* 3D-spheroid assay, we demonstrate that TIMP-2 suppressed spheroid expansion over the course of the four-day experiment in both TNBC cell lines tested, JygMC(A) and 4T1 (Figure 1A, Supplementary Figure 1A, available at *Carcinogenesis* Online). These findings are consistent with previous reports that show TIMP-2 inhibits growth factor-stimulated cell growth and invasion in a variety of primary (endothelial, fibroblasts) and tumor cell assays (14,25–27). Similarly, these studies have characterized TIMP-2 modulation of the EMT associated with the invasive phenotype. This prompted us to examine TIMP-2 effects on expression of transcription factors that are critical to the changes in gene expression associated with the EMT. Interestingly, we observed that TIMP-2 treatment of both TNBC cell lines, JygMC(A) and 4T1, demonstrated a trend toward suppression of the mesenchymal maker vimentin, as well as reduction in expression of the transcription factors SLUG and zinc-finger E-box (ZEB1), compared to untreated control cells under identical stimulated growth conditions (Supplementary Figure 1B, available at *Carcinogenesis* Online). This suggests that TNBC tumor cell growth and invasion are modulated by exogenous TIMP-2 treatment and that this effect may be mediated by suppression of the EMT drivers, such as SLUG, SNAIL, and ZEB1.

Initial in vivo experiments

We conducted initial experiments (Exp#1–3) to establish the optimal TIMP-2 concentrations and perform statistical power analysis of cohort size (see Supplementary Materials, Statistical considerations, available at *Carcinogenesis* Online). In Exp #1 and Exp #2, Figure 1B, bilateral tumor implants on five mice per experimental group received TIMP-2 doses ranging from 50 to 200 µg/kg/day starting on day 10 post tumor cell inoculation. These experiments demonstrated TIMP-2-dependent suppression of primary tumor growth. TIMP-2 doses of 50 and 200 µg/kg/day showed maximal primary tumor growth inhibition of ~42–50%, compared to vehicle controls ($^{**}P < 0.01$), whereas treatment with 400 µg/kg/day treatment did not show significant slowing of tumor growth. However, no significant change in body weight was observed in any of the treatment groups throughout the study duration, Supplementary Figure 1C, available at *Carcinogenesis*

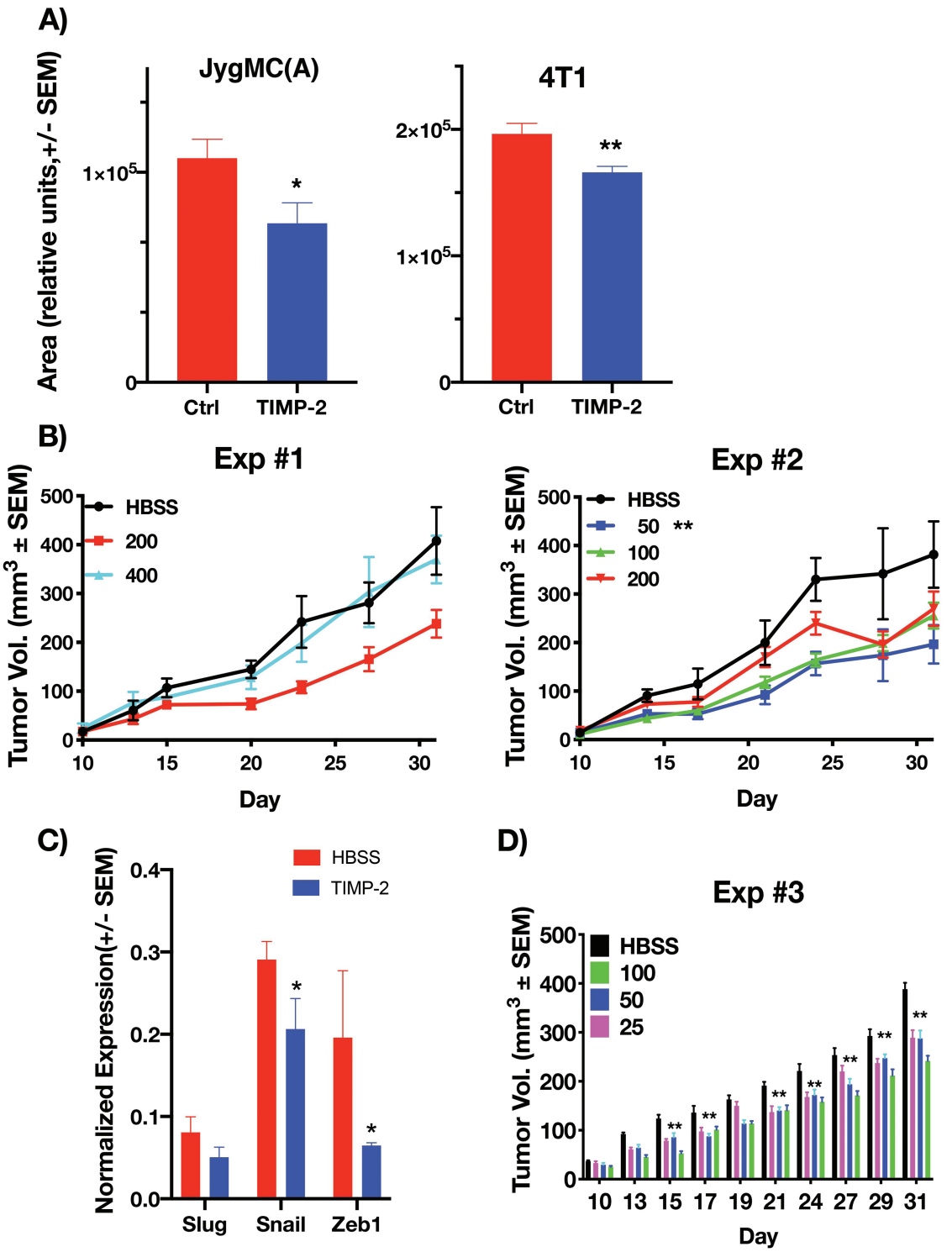

Figure 1. Initial experiments established TIMP-2 *in vitro* effects on TNBC cell line growth and invasion, as well as optimal TIMP-2 concentration and animal numbers from statistical power analysis. **(A)** Spheroid assays for TIMP-2 *in vitro* effects on growth/invasion of TNBC cell lines ($n = 3$). TIMP-2 treatment (1 μg/ml) results in significant reduction (*$P < 0.05$) in 3D growth of tumor cell spheroids on Culltrex basement membrane extract in both JygMC(A) and 4T1 breast cancer cell line cultures. **(B)** Experiments #1–2 (5 mice/group) revealed TIMP-2 concentrations ranging from 50 to 200 μg/kg/day were sufficient to statistically suppress primary tumor growth by 38–50%. **(C)** Immunoblot analysis of EMT driver transcription factor expression. Analysis of tumor lysates of vehicle control and 100 μg/kg/day TIMP-2-treated mice (Experiment #2) was performed in triplicate (three individual 1° tumor from different subjects). Analysis of SLUG, SNAIL, and ZEB1 expression was performed in triplicate. Integrated band densities were normalized to glyceraldehyde 3-phosphate dehydrogenase (loading control). Comparison between normalized expression levels in TIMP-2 and HBSS vehicle controls demonstrates a significant reduction in SNAIL and ZEB1 expression with a similar trend in SLUG expression. **(D)** Experiment #3 (10 mice/group) revealed significant inhibition of tumor growth with a TIMP-2 concentration as low as 25 μg/kg/day.

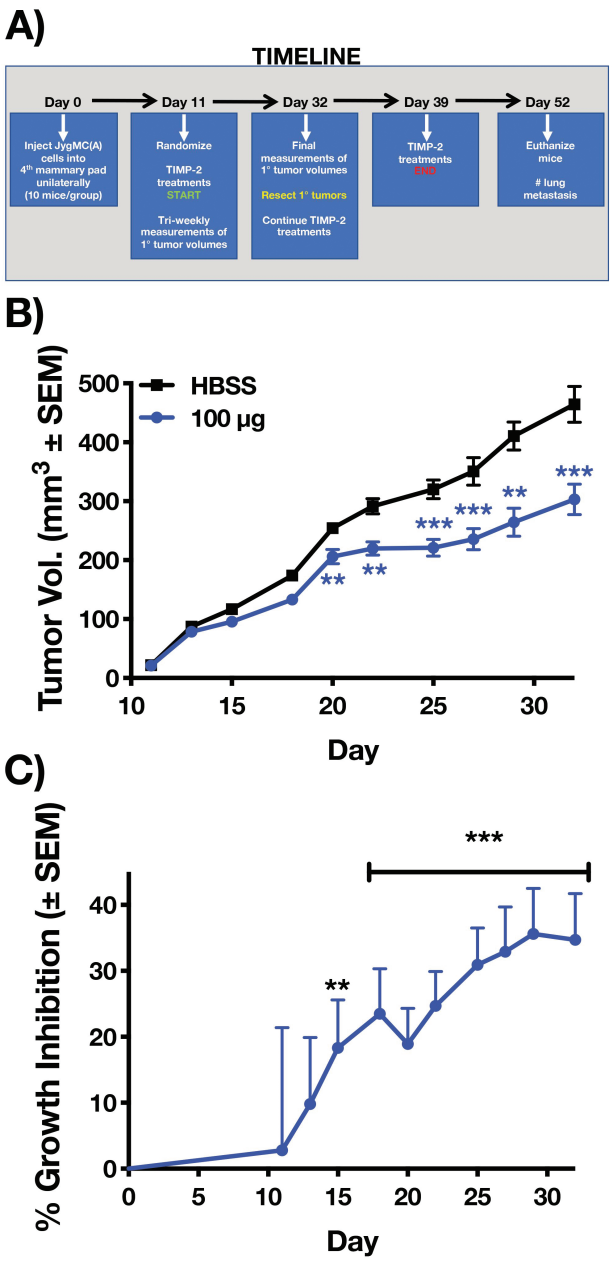

Figure 2. Experimental timeline of TIMP-2 treatment and tumor measurements. (**A**) Timeline of experiment. JygMC(A) tumors initiated in 20 female *nu/nu* mice by injection of 5 × 10^4 cells/mouse (20 µl) into the 4th inguinal mammary fat pat on day 0. Mice were randomized into two groups based on 1° tumor volume before initiation of daily i.p. injections of either vehicle control (HBSS) or 100 µg/kg/day TIMP-2 on day 11 and continued through day 39. Primary tumors were resected on day 32, mice euthanized on day 52. (**B**) Growth curve of caliper measurements shows significant reduction of tumor growth in TIMP-2-treated mice (blue) compared to controls (red) starting 15 days post tumor cell inoculation. (**C**) Maximum tumor growth inhibition in TIMP-2-treated cohort was observed on day 29 and began to plateau at ~36% inhibition thereafter (**$P < 0.01$, ***$P < 0.001$, $n = 10$).

Online. H&E stains of lung, liver, and spleen tissues demonstrate unaltered histology in both control and TIMP-2-treated mice, Supplementary Figure 1D, available at *Carcinogenesis* Online. These studies suggested no evidence of systemic toxicity or weight loss associated with TIMP-2 treatment. The apparent loss of the tumor growth suppressive effect at the highest TIMP-2 level (400 µg/kg/day) indicates a dose ceiling for the therapeutic effect on primary tumor growth requiring further investigation.

We also examined the expression of transcription factors that drive EMT changes in primary tumor tissue from Experiment #2, as we did for TNBC *in vitro* tumor cell cultures (Supplementary Figure 1B), available at *Carcinogenesis* Online). As shown, the analysis of triplicate tumor samples from treated and control mice demonstrate a significant reduction in SNAIL and ZEB1 expression (*$P < 0.05$), with a similar trend in SLUG expression, following TIMP-2 treatment (100 µg/kg/day), Figure 1C. These findings suggest that similar to effects *in vitro*, systemic administration of TIMP-2 suppresses *in vivo* 1° tumor growth and local invasion required for increasing tumor volume. Furthermore, this outcome may be modulated through repression of transcription factors responsible for activation of the EMT thus reducing tumor invasion and metastasis.

In a third experiment (Exp #3, Figure 1D), tumor cells were injected unilaterally into the inguinal mammary fat pads (10 mice per group) and primary tumor growth followed for 31 days. Daily i.p. doses of TIMP-2 ranging for 25–100 µg/kg/day were initiated 10 days post tumor cell injection. Mean tumor volume measurements demonstrate a statistically significant, dose-dependent reduction (**$P < 0.01$) in 1° tumor growth with maximal growth inhibition on day 31 of ~38%. This model of unilateral tumor development is more consistent with clinical experience and is not influenced by confounding multiple tumor sites, or excessive 1° tumor burdens. The results provide a clear demonstration of the suppressive effects of TIMP-2 on primary tumor growth (see Supplementary material, Statistical Considerations, available at *Carcinogenesis* Online).

TIMP-2 inhibits 1° TNBC growth via alteration in phenotype and vascular permeability

Based on our initial findings, we selected a dose of 100 µg/kg/day to further evaluate the effect of TIMP-2 on primary tumor growth, phenotype, vascular integrity, and pulmonary metastasis following unilateral tumor cell injections using 10 mice/group. A timeline for these experiments shows that 1° tumors were initiated on day 0, on day 11, animals were randomized into two groups based on initial tumor volumes before TIMP-2 and vehicle control injections were initiated, then 1° tumors were resected on day 32. TIMP-2 treatment was continued 1 week following 1° tumor resections (terminated on day 39). All mice were euthanized on day 52 (13 days post-termination of TIMP-2 treatment), and whole lungs were obtained at necropsy.

Tumor volume measurements revealed a significant reduction starting 3 days postinitiation of TIMP-2 treatment compared to vehicle controls and continued until removal of primary tumors on day 32 (***$P < 0.001$), Figure 2B. Percent growth inhibition also showed differences starting 3 days after the start of TIMP-2 treatment (day 15) and reached a maximum value of 36% at day 29 (***$P < 0.001$), Figure 2C.

TIMP-2 suppression of EMT phenotype

TNBCs are distinguished both histologically and immunohistochemically by basal-like features indicative of a mesenchymal phenotype that is associated with the EMT as well as invasion and metastasis (28–31). We have previously reported that JygMC(A) cells demonstrate a basal-like, mesenchymal phenotype in culture and that mammary xenografts

histologically exhibit two distinct morphologies, i.e. undifferentiated adenocarcinoma or spindle-shaped basal/mesenchymal appearance (20). Interestingly, histology of tumors from TIMP-2-treated mice resembled that of undifferentiated carcinoma without basal/mesenchymal appearance, and immunochemical staining for epithelial (cytokeratin-18) versus basal (keratin 14, K14) and mesenchymal (vimentin, Vim) markers demonstrated a significant reduction in basal/mesenchymal markers in the 1° tumors from TIMP-2-treated mice, Figure 3A. Scoring of 1° tumor staining confirmed that TIMP-2-treated mice showed a significant increase in CK-18, along with decreased K-14 and Vim expression observed in TIMP-2-treated mice (Figure 3A and B, $^{**}P < 0.01$, $^{***}P < 0.001$). These findings suggest a change in gene expression associated with a more differentiated phenotype and suppression of the EMT process in TIMP-2-treated tumors, consistent with the reduced expression of EMT-driver transcription factors observed previously (Figure 1C).

TIMP-2 treatment promotes vascular normalization

Enhanced type IV collagen deposition and enhanced pericyte coverage are phenotypic changes that have been associated

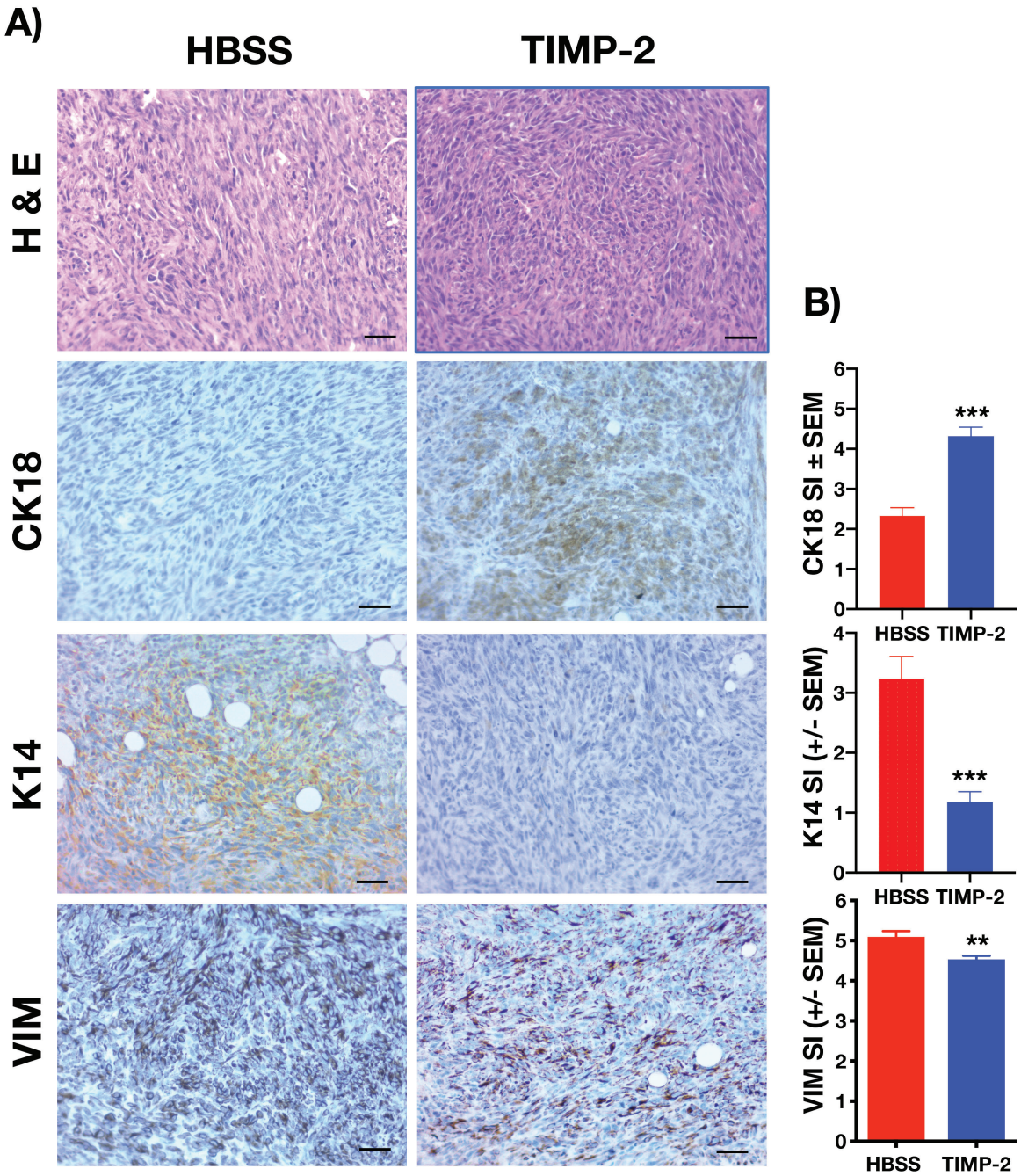

Figure 3. TIMP-2 treatment alters JygMC(A) TNBC phenotype and EMT profile. (**A**) H and E immunostaining of epithelial (CK18), basal (K14), and mesenchymal (Vim) markers in sections mammary tumors from HBSS (vehicle control) and TIMP-2-treated mice. (**B**) Graphs representing mean (±SEM) IHC staining index in TIMP-2-treated tumors showing increased epithelial (CK-18) and a reduction in basal/mesenchymal markers CK-14 and Vim ($^{**}P < 0.01$, $^{***}P < 0.001$, $n = 10$; bar = 50 µm).

with reduced vascular permeability and enhanced delivery of chemotherapeutic agents following antiangiogenic therapy. This process has been defined as 'vascular normalization' (32). We have previously demonstrated that TIMP-2 reduces endothelial permeability in response to VEGFA stimulation *in vitro* (15). Dual immunofluorescence revealed no difference in overall CD31⁺ microvessel density. However, enhanced type IV collagen continuity was observed in association with CD31⁺ endothelia in tumors harvested from TIMP-2-treated mice, Figure 4A. Image analysis revealed that type IV collagen mean fluorescence intensity was significantly increased in the TIMP-2 treatment group (***$P < 0.001$). These structural features translate to functional significance as examination of rhodamine B-labeled dextran extravasation demonstrated a reduction in vascular leakage in TIMP-2-treated mice compared to controls, Figure 4B (**$P < 0.01$). Collectively, these findings provide evidence that TIMP-2 contributes to the 'normalization' of tumor vasculature *in vivo*, consistent with previously reported TIMP-2 antiangiogenic activity (25,33,34).

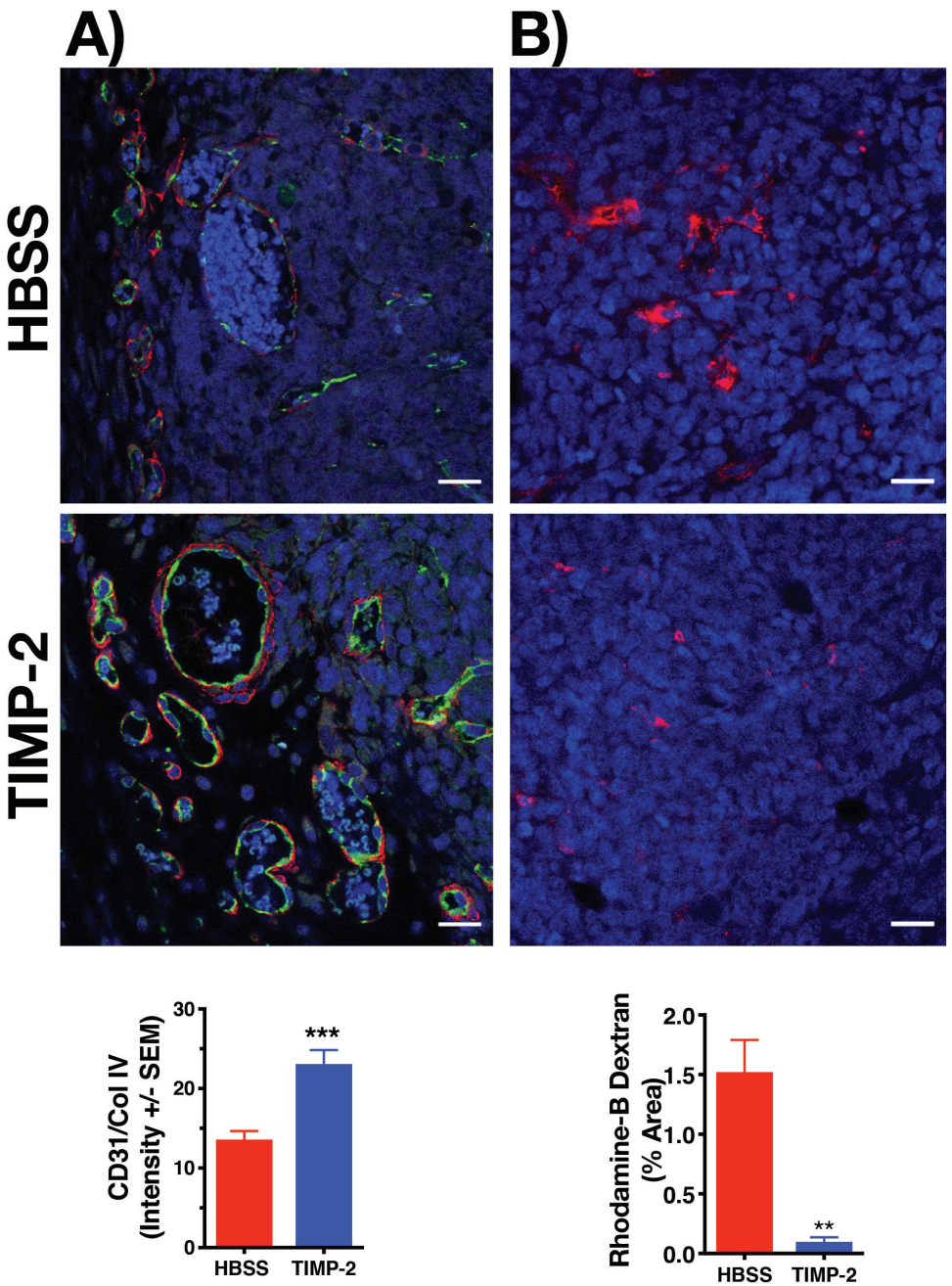

Figure 4. TIMP-2-treatment enhances 'vascular normalization'. (**A**) Confocal images of dual IF show enhanced endothelial cell coverage (CD31, green) and type IV collagen deposition (Col IV, red) in tumor vasculature of TIMP-2-treated mice compared to HBSS controls (bar = 20 μm). Graphical presentation of quantified Col IV staining (mean ± SEM, ***$P < 0.001$). (**B**) A significant reduction in extravasated rhodamine B-labeled dextran (red) was observed in TIMP-2-treated tumors compared to controls (bar = 20 μm). Graph represents percent (%) area of rhodamine B leakage quantified by Image J software in 6–10 confocal images per experimental group (mean ± SEM, **$P < 0.01$).

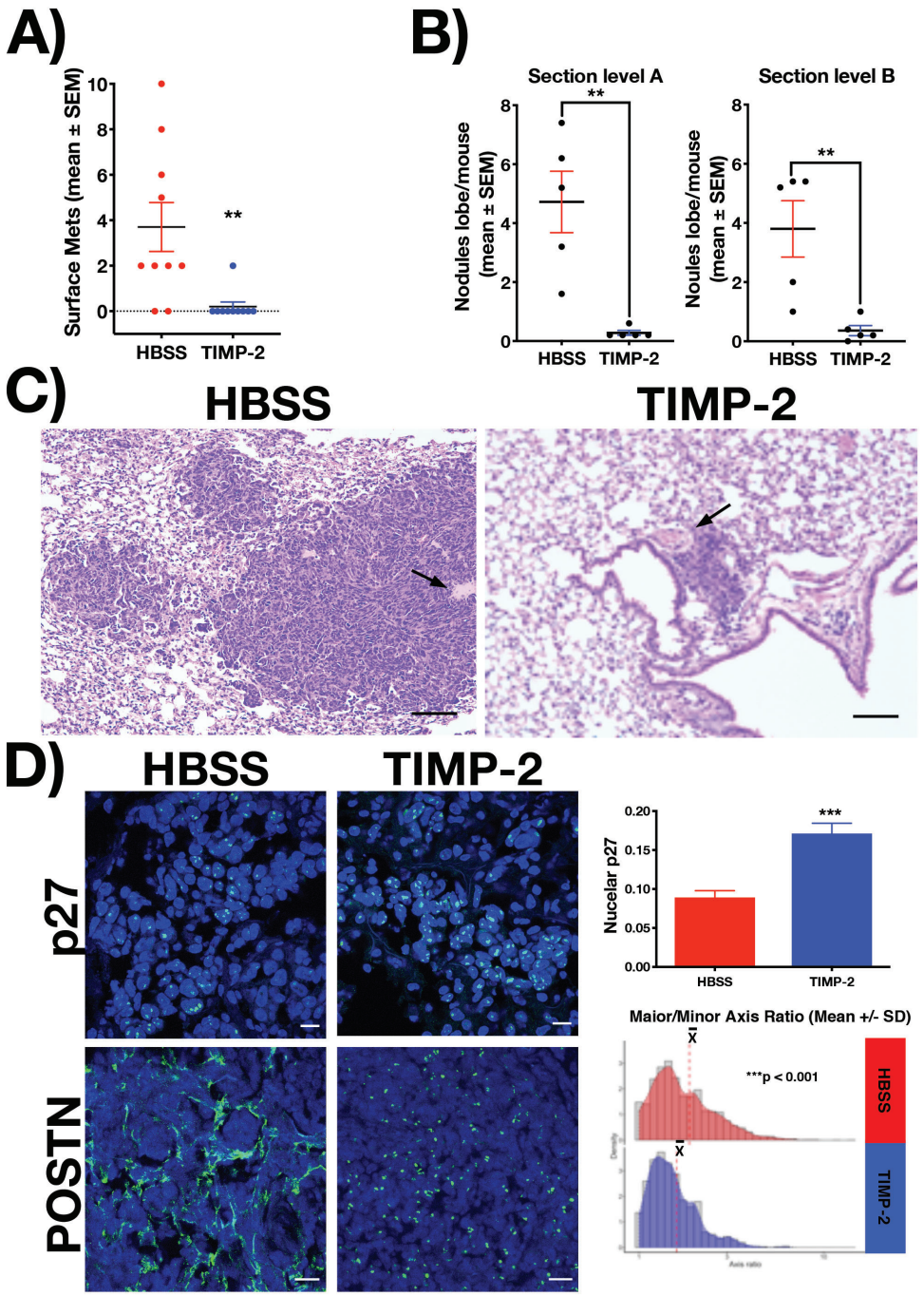

Figure 5. TIMP-2-treatment reduces pulmonary metastasis 15 days posttreatment. (**A**) Scatter plot represents reduction in surface lung nodules in TIMP-2-treated mice compared to vehicle controls ($n = 10$, two-tailed, unpaired t-test, $^{**}P < 0.01$). (**B**) Scatter plots show decreased number of metastatic tumor nodules per lobe in two levels of H and E stained whole lung step sections 100 µm apart (two-tailed, unpaired *t*-test, *P* values shown, $n = 5$). (**C**) Photomicrographs of metastatic lesions in lungs of TIMP-2-treated mice compared to controls illustrate decreased size of metastasis and metastatic tumor burden. Metastases in both groups are vasculocentric consistent with hematogenous dissemination (arrows, H and E, bar = 50 µm). (**D**) Confocal images illustrate enhanced nuclear p27 expression in lung metastatic tumors of TIMP-2-treated mice compared to HBSS control animals (upper panel) ($^{***}P < 0.001$, unpaired *t*-test). A dramatic difference in POSTN staining was observed in lung metastatic tumor stroma of TIMP-2-treated animals which demonstrated small, rounded punctate regions compared to an extended pericellular distribution pattern of expression in untreated controls (lower panel). Quantification of POSTN staining revealed a significant difference in mean axis ratios, consistent with linear pattern in tumor from control mice (Mann–Whitney, two-tailed test, bar = 10 µm).

TIMP-2 treatment reduces metastatic frequency and growth

Examination of whole lungs resected upon termination of the experiment at day 52 revealed a large reduction (>92%) in pulmonary metastases shown in Figure 5A ($^{**}P < 0.01$). These findings were confirmed by histological assessment of the average number of tumor nodules per lung lobe tabulated from two H&E stained whole lung step sections 100 µm apart, Figure 5B. Also, photomicrographs of representative H&E lung sections suggest reduced size of metastasis and extent of tumor burden

in lungs of TIMP-2-treated mice, as well as the perivascular localization for these metastatic foci, Figure 5C. These observations suggest that TIMP-2 treatment, in addition to altering 1° tumor growth and phenotype, significantly alters metastatic lung colonization and/or outgrowth in the JygMC(A) model of TNBC.

In contrast to the differences observed in the primary tumor xenografts, pulmonary metastatic foci in the lungs of both TIMP-2 and vehicle control-treated mice both showed morphology typical of poorly differentiated adenocarcinoma (Supplementary Figure 2, available at *Carcinogenesis* Online). In addition, statistical comparisons of immunophenotyped scoring of EMT markers (K14, Vim) expression in lung metastasis failed to demonstrate the differences observed in primary tumor staining. These findings are consistent with loss of the EMT phenotype, so called mesenchymal-to-epithelial reversion, as previously reported in the JygMC(A) model (20). To further elucidate the potential effects of TIMP-2 on tumor cells in the metastatic foci, we examined markers associated with tumor growth and metastasis, as well as ECM alterations associated with metastasis formation and outgrowth.

Alteration of phenotypic markers of cell growth and PMN formation in pulmonary metastasis

The CDK inhibitor p27, an effector of TGF-β growth arrest, is functionally impaired in human cancers by multiple mechanisms, such as phosphorylation, proteome degradation, and/or diminished *de novo* synthesis (35,36). Phosphorylation of p27 enhances cytoplasmic localization, is frequently the result of PI3K-pathway activation, and both are associated with increased metastasis and poor outcome in human breast cancers (37,38). To further investigate the apparent TIMP-2 effect on the growth of pulmonary metastasis, we examined expression and nuclear localization of p27 in pulmonary metastasis from JygMC(A) tumors in TIMP-2-treated and control mice. The results clearly show enhanced nuclear localization following TIMP-2 treatment, Figure 5D (***$P < 0.001$).

Periostin (POSTN) is a component of the extracellular matrix that is associated with metastasis formation (39). POSTN is induced in lung stroma by infiltrating cancer cells but is not observed in alveolar stroma of normal lung. We analyzed the extent and pattern of POSTN accumulation in JygMC(A) pulmonary metastasis by immunofluorescence staining. The results demonstrate a distinct pattern of pericellular deposition of POSTN in the pulmonary metastasis from control animals but not in TIMP-2-treated mice, Figure 5D. Quantification demonstrates an enhanced punctate pattern in the TIMP-2-treated mice with highly significant differences in mean axis ratio. Together, these findings examining p27 and POSTN expression/localization in tumor metastasis suggest that TIMP-2 treatment alters gene expression at secondary tumor sites that result in changes that do not support metastatic outgrowth.

TIMP-2 treatment alters global gene expression at the PMN

Uninvolved lung tissues (no evidence of tumor involvement) were obtained from TIMP-2-treated and control mice at the termination of the experiment on day 52, Figure 2A. The transcriptional profiles of these tissue samples were examined by total RNA sequencing as well as immune-blot analyses. PCA of these samples reveals distinct clustering of the TIMP-2-treated samples but only modest clustering of the controls (Figure 6A). However, when the frequency of metastasis (data Figure 5A) was layered over the PCA, two distinct clusters are observed that highlight the group with few ($n \leq 2$) or no metastasis versus those with greater number of metastasis in other areas of the lungs (Figure 6A). While suggesting that the presence of metastatic foci results in altered gene expression in uninvolved lung, it is important to recognize that gene-specific analysis (GSA) of EM normalized RefSeq gene counts (Partek® Flow®'s) highlights a total of 302 upregulated and 114 downregulated genes following TIMP-2 treatment ($P < 0.05$, false discovery rate <0.5) (Supplementary Data Set 1, available at *Carcinogenesis* Online). These gene clusters are clearly highlighted in the Pearson's clustered heatmap (Figure 6B, Gene Cluster 1, 114 downregulated, Gene Cluster 2, 302 upregulated). The data are highly significant in that the prominent segregation occurs irrespective of the presence of metastatic foci and correlates directly with systemic administration of TIMP-2. These findings suggest, in confluence with the changes associated with 'vascular normalization' described above, that systemic administration of TIMP-2 not only directly alters tumor cell growth and invasion (*in vitro* and *in vivo* data) but also influences host cell responses that are opposed to tumor growth and dissemination.

Gene set enrichment analysis of these GSA-identified gene lists highlighted pathways and upstream regulators of relevance to enhanced metastasis formation, Figure 6C and D. Specifically, the reduced activity of the Wnt/β-catenin pathway (involved in EMT and downstream of POSTN) and upstream regulators of PI3K are notable in that they relate directly to the changes previously observed in p27 and POSTN expression in pulmonary metastasis, Figure 5D (37,39). Also, these global RNASeq studies identified reduced activity in upstream regulators of the ERK 1/2, TGFβ1, and β-catenin (LEF1) pathways that were confirmed by immunoblot analysis at the protein level, Figures 6E and Supplementary Figure 3, available at *Carcinogenesis* Online. The immunoblot results demonstrate decreased p-ERK, p-Stat5, PDGFR- β LEF1, and SLUG levels in uninvolved lung tissues following TIMP-2 treatment. These findings suggest that TIMP-2 treatment suppressed a gene expression profile associated with an 'activated' phenotype at the PMN necessary for tumor cell colonization and successful outgrowth. The findings of a potential systemic effect of TIMP-2 are surprising in that they appear to persist in nontumor containing lung tissues two weeks after discontinuation of TIMP-2 treatment.

Discussion

The architecture and function of the extracellular matrix of normal tissues is well characterized as a dynamic niche that suppresses tumor development, invasion, and metastasis. Tumor cell-mediated changes in this microenvironmental 'barrier' resulting in an abnormal ECM, both at the primary tumor site and distant organ sites (premetastatic/metastatic niche), are necessary for tumor development and progression (6,7,9,40). MMPs are primary effectors of ECM remodeling associated with tumor progression and their inhibitors, TIMPs, are principal regulators of their proteolytic activity (12,27,41). Previous studies demonstrate that TIMP-2 is expressed in most normal tissues and is readily detectable even in the absence of significant MMP expression. These findings suggest that TIMP-2 may possess homeostatic functions independent of its MMP-inhibitory activity. Indeed, such MMP-independent functions have been characterized for several members of the TIMP family, including TIMP-2 (12,27,41). These observations have led us to posit that during tumor progression there is a shift in TIMP function from the MMP-independent functions that maintain homeostasis in normal tissues, toward a more direct role in regulation of MMP

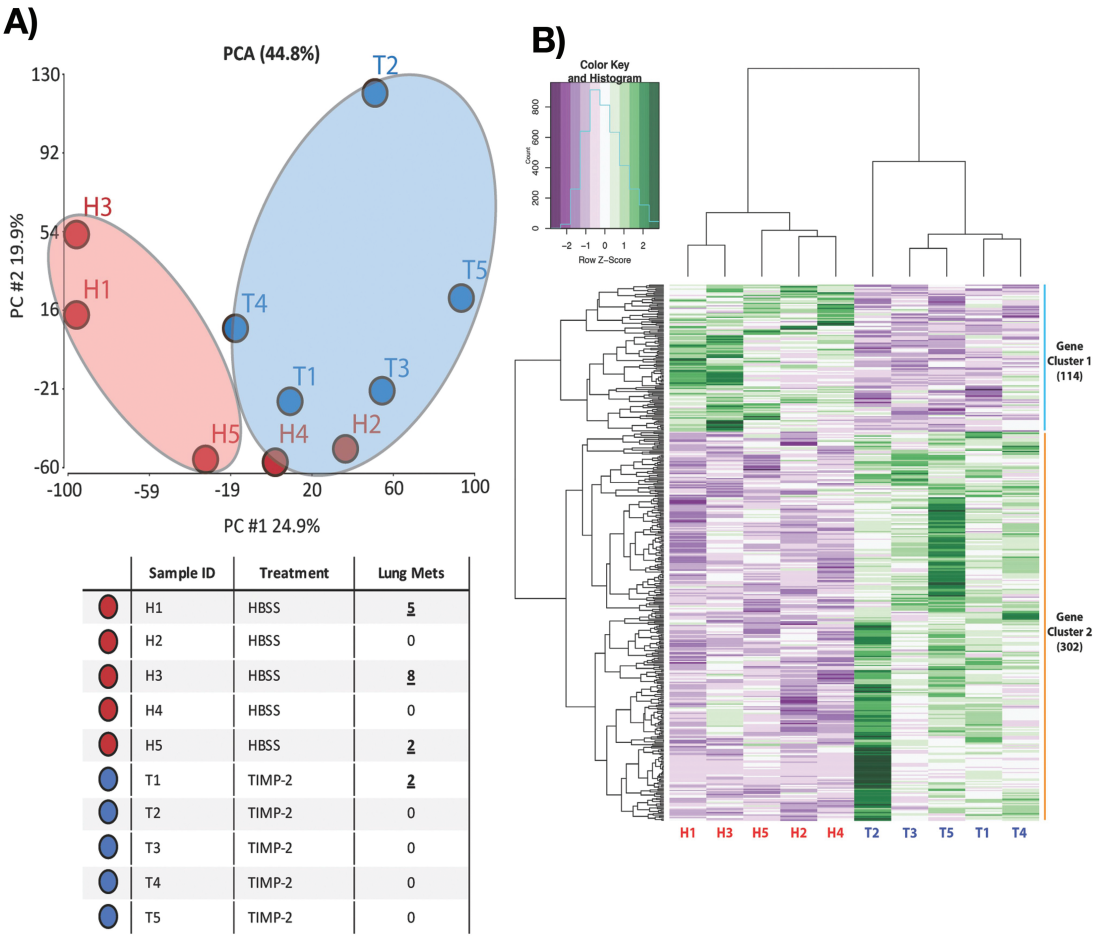

	Sample ID	Treatment	Lung Mets
●	H1	HBSS	5
●	H2	HBSS	0
●	H3	HBSS	8
●	H4	HBSS	0
●	H5	HBSS	2
●	T1	TIMP-2	2
●	T2	TIMP-2	0
●	T3	TIMP-2	0
●	T4	TIMP-2	0
●	T5	TIMP-2	0

C)

Ingenuity Canonical Pathways

Pathway	p-Value	Activation	Genes Involved
Epithelial Adherens Junction Signaling	0.002		ACTN2,EGF,TUBA1C,LEF1,TUBB4A,MYH11,ACTC1,Tcf7
Hepatic Fibrosis	0.002		COL24A1,MMP13,EGF,IGFBP5,COL6A5,MYH11,FASLG,CCR7,COL6A6
Agranulocyte Adhesion and Diapedesis	0.010		AOC3,CXCL13,IL1RN,MMP13,MYH11,MMP12,ACTC1,C5
Cytotoxic T Cell-mediated Apoptosis	0.013		PRF1,HLA-A,FASLG
Calcium Signaling	0.014	↑	CACNA1G,GRIN2B,CACNA1B,RYR2,TRDN,MYH11,ACTC1, CASQ2
ILK Signaling	0.032	↑	RHOV,ACTN2,PPP2R2B,MAPK10,LEF1,MYH11,ACTC1
Atherosclerosis Signaling	0.046		PLA2G2D,IL1RN,MMP13,SERPINA1,TPSAB1/TPSB2
Wnt/β-catenin Signaling	0.050	↓	SFRP2,SOX21,CDH3,PPP2R2B,LEF1,Tcf7

D)

Upstream Regulator Analysis

Regulator	Type	Activation	Network Coverage (%)	
ERK1/2	Kinase	↓	6.16	Growth Factor Signaling
VEGFA	Growth factor	↓	9.34	
ERBB2	Kinase	↓	7.49	
TGFB1	Growth factor	↓	6.61	
EGF	Growth factor	↓	6.51	
IL1B	Cytokine	↓	7.34	Inflammation
TNF	Cytokine	↓	7.05	
PI3K	Kinase	↓	6.90	
IL6	Cytokine	↓	6.85	
STAT1	Transcription regulator	↓	6.23	
MYC	Transcription regulator	↓	7.27	Transcriptional Regulation
β-catenin	Transcription regulator	↓	5.59	

p<0.0001 for all Regulators listed

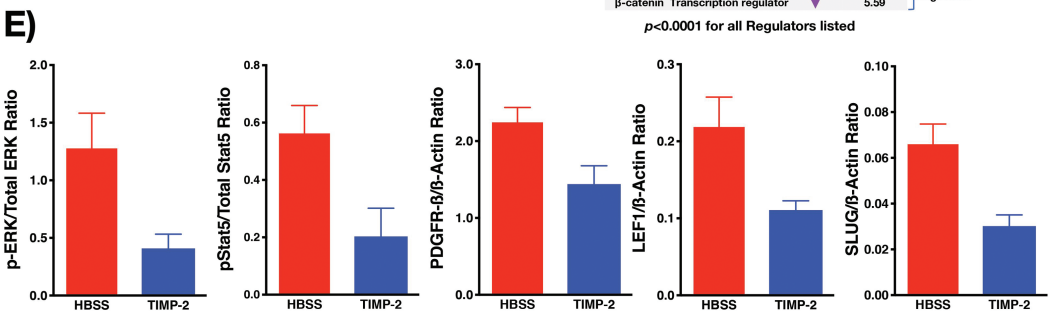

Figure 6. Gene expression profiles of uninvolved lung tissue from TIMP-2-treated and vehicle control tumor bearing mice. (**A**) Sample information and principle component analysis of normalized total RNA sequencing data from dissected, tumor-free lung tissue of study mice with daily intraperitoneal injection of 100 μg/kg/day TIMP-2 or HBSS for 28 Days (Day 11 through Day 39, see Figure 2A) followed by 13 days without treatment (Day 39 through Day 52, see Figure 2A). (**B**) Clustered heatmap depicting the Pearson's correlation metric with complete linkage between RNA sequencing samples and GSA significant genes ($P < 0.05$, false discovery rate 0.5). (**C**) and (**D**) Selected canonical pathways and upstream regulators highlighted from gene set enrichment analysis of significant gene changes using Ingenuity Pathway Analysis. (**E**) Graphic representation of immunoblot analysis of protein expression in TIMP-2 and control treated uninvolved lung tissues. Results of immunoblotting demonstrate significant downregulation of p-ERK (relative to total ERK), pSTAT5 (relative to total STAT5), as well as PDGFR- β, LEF7 and Slug protein expression following TIMP-2 treatment compared to vehicle controls (*-*$P < 0.05$, **$P < 0.01$, after normalization to β -actin or total nonphosphorylated protein levels, See Supplementary Figure 2, available at *Carcinogenesis* Online). These findings confirm the results of transcriptome profiling demonstrating reduced activation of pathways involved in PMN formation and/or metastatic potential.

activity and inhibition of cellular invasion (12,27,41,42). However, implicit in this model of TIMP-2 function is the concept that restoration of MMP-free TIMP-2 levels may function to re-establish normal tissue functions as well as suppress invasive and metastatic progression in cancer.

Previous studies have attempted to test this hypothesis using models in which TIMP-2 is overexpressed in tumor cells, in part due to the lack of sufficient recombinant protein. These studies suggest TIMP-2 may inhibit primary tumor growth and metastasis, via mechanisms that suppress tumor growth, angiogenesis, and EMT independent of MMP inhibitory activity (14,43–45). However, possible TIMP-2 effects on uninvolved, stromal tissues at sites of metastatic outgrowth have not be examined. To further test this hypothesis, we utilized the JygMC(A) model of TNBC, extensively characterized as highly representative of breast cancer progression in humans, to determine if systemic administration of MMP-free, exogenous TIMP-2 via intraperitoneal injection would modulate tumor growth and metastasis (20).

TIMP-2 treatment not only reduced 1° tumor growth by as much as 35–50% but also promoted a more carcinomatous versus basal phenotype that was validated by reduced expression of transcriptional drivers of EMT (SLUG, SNAIL, and ZEB1), as well as increased epithelioid marker CK-18 staining, and concomitant reduction in basal mesenchymal markers (K-14 and Vim). These findings are consistent with previous reports describing the suppressive effects of TIMP-2 on primary tumor growth, via forced tumor cell expression in cancer cell lines (14). Furthermore, the observed phenotypic changes are in agreement with previous reports describing suppression of the EMT and oncogenic side-populations (cancer stem cells) in human lung cancer cell lines (43,46).

TIMP-2 is reported to inhibit angiogenesis and promote vascular normalization via an integrin-mediated mechanism that involves an Shp1-p27-Rb signaling to suppress mitogen stimulation and enhance VE-cadherin cytoskeletal association (15,25). In the present study, we specifically examined the effect of TIMP-2 on 'vascular normalization' in 1° mammary tumors. The result of these immunofluorescence studies strikingly demonstrates a significant increase in $CD31^+$ endothelial cells associated with increased type IV collagen deposition in the subendothelial basement membrane of tumor-associated vessels of TIMP-2-treated mice, which is also associated with a marked reduction in vascular permeability. These findings of both reduced 1° tumor growth and apparent suppression of EMT markers suggest that these apparent direct effects on tumor cells combined with the antiangiogenic activity of TIMP-2 result in reduced metastatic potential. These observed effects at the 1° tumor site may directly contribute to the observation of a greatly reduced frequency of pulmonary metastasis in TIMP-2-treated mice; however, we also considered TIMP-2 effects downstream at sites of metastasis formation.

In the present study, we observed a highly significant reduction of >92% in the frequency and size of pulmonary metastasis in the TIMP-2-treated cohort compared with vehicle control. The EMT in TNBC is associated with canonical Wnt/β-catenin-signaling and an increased risk of metastasis (47–49). However, metastasis formation is often associated with the reversal of EMT at the secondary site, so called mesenchymal-to-epithelial transition, that has been extensively characterized in the JygMC(A) model (20). However, pulmonary metastatic foci in the lungs of both TIMP-2- and HBSS-treated mice showed similar morphology typical of poorly differentiated adenocarcinoma and no significant differences in basal/mesenchymal marker expression. Thus, we looked to other metastasis-associated markers to examine the effects of TIMP-2 on metastatic tumor cells.

The CDK inhibitor p27 is functionally altered via phosphorylation, proteasome processing, or diminished *de novo* synthesis in most cancers, including TNBC (35,36). Enhanced phosphorylation of p27 prevents nuclear import, blocks growth suppressive activity, and is associated with increased metastasis and poor outcome in human breast cancers (38). Our results clearly show enhanced nuclear localization in tumor cells at sites of pulmonary metastasis following TIMP-2 treatment. It has been previously reported that in fibroblasts and endothelial cells, TIMP-2 treatment results in increased *de novo* p27 expression and enhanced nuclear localization resulting in the suppression of cell growth (50).

We posit that the effects of TIMP-2 treatment on tumor cells within the primary tumor resulting in a maximal ~36–50% inhibition of growth, as well as 'normalization' of the tumor vasculature contribute to the observed reduction in the frequency of pulmonary metastasis. Furthermore, we demonstrate evidence of a direct effect of TIMP-2 on tumor cell growth in the pulmonary metastasis, via increased p27 nuclear localization, that can mitigate tumor cell growth at these secondary sites. This may contribute to the reduction in size of the metastatic lesions observed in TIMP-2-treated mice compared to controls. However, none of these findings rule out potential effects of systemically administered TIMP-2 on the local tissue microenvironment, specifically at sites of metastasis formation.

Several markers indicative of ECM preparation of this 'soil' for ensuing tumor cell outgrowth and metastasis formation have been identified. For example, tumor cell induction of periostin (POSTN) expression at the secondary site is among a growing number of penultimate markers that appear critical for pulmonary colonization by breast cancer (6,7,39,51). In metastatic lesions from TIMP-2-treated mice, we observed a clear disruption of the pericellular, stromal localization of POSTN distribution that was readily apparent in vehicle control-treated animals. Furthermore, these findings suggest the possibility that TIMP-2 treatment results in changes in host tissue gene expression, disrupting pathways essential for metastasis formation. To address this issue, we examined global gene expression profiles in posttreatment, uninvolved lung tissues from TIMP-2, and vehicle control-treated mice, collected 15 days after discontinuation of TIMP-2 treatment.

RNA-sequencing experiments were performed to characterize differences in gene expression profiles in the nontumor-bearing, uninvolved lung tissues of vehicle control and TIMP-2-treated mice. While the PCA findings alone may suggest that the presence of metastasis influences transcriptome expression, our findings utilizing GSA analysis demonstrate that there was a clearly defined segregation in the pattern of gene expression among lung tissues from TIMP-2-treated and control mice independent of the presence of metastasis. Furthermore, these data sets align directly with systemic TIMP-2 treatment despite the fact that TIMP-2 administration was completed 13 days prior to tissue collection. The emerging gene profiles following TIMP-2 treatment show suppression of gene subsets that have been critically associated with formation of breast cancer metastasis. In addition to disruption of the distinct pattern of POSTN staining in metastatic lesions in vehicle control lungs, not observed in the TIMP-2 treatment cohort, our data show activation of Wnt signaling, which reportedly occurs downstream of POSTN and supports outgrowth of metastatic tumor cells (39). Interestingly, pathway analysis of the GSA-identified gene lists comparing control versus TIMP-2-treated lung tissues demonstrates a significant down regulation of Wnt/β-catenin signaling (Figure 6C), in accordance with the reduced frequency

of lung metastasis following TIMP-2 treatment. Similarly, Upstream Regulator Analysis identified gene sets such as PI3K and β-catenin that are reportedly involved in either p27, POSTN, and/or EMT regulation (Figure 6D). Since these gene expression changes were observed in histologically normal tissue, we suggest that the antitumor, stromal 'normalizing' effects of administered exogenous TIMP-2 are both direct, as evidenced from prior studies, and systemic (14,43).

In summary, our study confirms previous findings demonstrating that exogenously administered TIMP-2 induces altered gene expression resulting in suppression of EMT, a reduction in vascular permeability, and inhibition of 1° tumor growth by >35%. The present report extends these findings to show that exogenous TIMP-2 treatment initiated 10 days after tumor cell inoculation results in >92% inhibition of pulmonary metastasis when assessed 2 weeks after cessation of TIMP-2 injections. Furthermore, analysis of metastatic tumor foci for CDK inhibitor expression shows increased p27 nuclear staining associated with reduced cell growth. In addition, TIMP-2 treatment reduced POSTN extracellular deposition that is strongly correlated with PMN formation in breast cancer. Finally, RNA sequencing analysis of gene expression in noninvolved lung tissues demonstrates a pattern of decreased transcriptome activity in cell signaling pathways involved in EMT, metastatic colony formation, and stromal activation associated with increased tumor metastasis. These findings are consistent with our hypothesis that the protease-independent (and MMP inhibitory) activities of TIMP-2 may function to repair stromal homeostasis and prevent changes involved in formation of the lung metastasis in TNBC. This study is the first to demonstrate that systemic administration of an ECM constituent from normal stromal tissues results in suppression of tumor growth and metastasis that could be exploited in the development of novel therapeutic strategies for the treatment of TNBC and possibly other cancers.

Supplementary material

Supplementary data are available at *Carcinogenesis* online.

Funding

This work was supported by the National Institutes of Health, National Cancer Institute, Center for Cancer Research Intramural Research Program [Project # ZIA SC009179-25].

Acknowledgements

We would like to thank the NIH Division of Veterinary Resources for their technical assistance.
Conflict of Interest Statement: None declared.

References

1. Paget, S. (1889) The distribution of secondary growths in cancer of the breast. *Lancet*, 133, 571–573.
2. Fidler, I.J. (2003) The pathogenesis of cancer metastasis: the 'seed and soil' hypothesis revisited. *Nat. Rev. Cancer*, 3, 453–458.
3. Hanahan, D. *et al.* (2011) Hallmarks of cancer: the next generation. *Cell*, 144, 646–674.
4. Lambert, A.W. *et al.* (2017) Emerging biological principles of metastasis. *Cell*, 168, 670–691.
5. Biswas, S.K. (2015) Metabolic reprogramming of immune cells in cancer progression. *Immunity*, 43, 435–449.
6. Peinado, H. *et al.* (2017) Pre-metastatic niches: organ-specific homes for metastases. *Nat. Rev. Cancer*, 17, 302–317.
7. Sceneay, J. *et al.* (2013) The pre-metastatic niche: finding common ground. *Cancer Metastasis Rev.*, 32, 449–464.
8. Liotta, L.A. *et al.* (1991) Cancer metastasis and angiogenesis: an imbalance of positive and negative regulation. *Cell*, 64, 327–336.
9. Lu, P. *et al.* (2012) The extracellular matrix: a dynamic niche in cancer progression. *J. Cell Biol.*, 196, 395–406.
10. Brew, K. *et al.* (2010) The tissue inhibitors of metalloproteinases (TIMPs): an ancient family with structural and functional diversity. *Biochim. Biophys. Acta*, 1803, 55–71.
11. Bourboulia, D. *et al.* (2010) Matrix metalloproteinases (MMPs) and tissue inhibitors of metalloproteinases (TIMPs): positive and negative regulators in tumor cell adhesion. *Semin. Cancer Biol.*, 20, 161–168.
12. Grünwald, B. *et al.* (2019) Recognizing the molecular multifunctionality and interactome of TIMP-1. *Trends Cell Biol.*, 29, 6–19.
13. Coussens, L.M. *et al.* (2002) Matrix metalloproteinase inhibitors and cancer: trials and tribulations. *Science*, 295, 2387–2392.
14. Bourboulia, D. *et al.* (2011) Endogenous angiogenesis inhibitor blocks tumor growth via direct and indirect effects on tumor microenvironment. *Am. J. Pathol.*, 179, 2589–2600.
15. Kim, S.H. *et al.* (2012) Antagonism of VEGF-A-induced increase in vascular permeability by an integrin α3β1-Shp-1-cAMP/PKA pathway. *Blood*, 120, 4892–4902.
16. Walsh, L.A. *et al.* (2012) Analysis of the MMP-dependent and independent functions of tissue inhibitor of metalloproteinase-2 on the invasiveness of breast cancer cells. *J. Cell Commun. Signal*, 6, 87–95.
17. Remillard, T.C. *et al.* (2014) Molecular mechanisms of tissue inhibitor of metalloproteinase 2 in the tumor microenvironment. *Mol. Cell. Ther.*, 2, 17.
18. Stetler-Stevenson, W.G. (2008) Tissue inhibitors of metalloproteinases in cell signaling: metalloproteinase-independent biological activities. *Sci. Signal*, 1, re6.
19. Lee, A. *et al.* (2018) Triple negative breast cancer: emerging therapeutic modalities and novel combination therapies. *Cancer Treat. Rev.*, 62, 110–122.
20. Castro, N.P. *et al.* (2015) Cripto-1 as a novel therapeutic target for triple negative breast cancer. *Oncotarget*, 6, 11910–11929.
21. Hiroishi, S. *et al.* (1995) Multiple metastases of mammary carcinoma cell lines isolated from feral mouse. *Cancer Lett.*, 92, 83–86.
22. Chowdhury, A. *et al.* (2017) Tissue inhibitor of metalloprotease-2 (TIMP-2): bioprocess development, physicochemical, biochemical, and biological characterization of highly expressed recombinant protein. *Biochemistry*, 56, 6423–6433.
23. Allred, D.C. *et al.* (1992) HER-2/neu in node-negative breast cancer: prognostic significance of overexpression influenced by the presence of in situ carcinoma. *J. Clin. Oncol.*, 10, 599–605.
24. Padua, D. *et al.* (2008) TGFbeta primes breast tumors for lung metastasis seeding through angiopoietin-like 4. *Cell*, 133, 66–77.
25. Seo, D.W. *et al.* (2003) TIMP-2 mediated inhibition of angiogenesis: an MMP-independent mechanism. *Cell*, 114, 171–180.
26. Seo, D.W. *et al.* (2006) Shp-1 mediates the antiproliferative activity of tissue inhibitor of metalloproteinase-2 in human microvascular endothelial cells. *J. Biol. Chem.*, 281, 3711–3721.
27. Stetler-Stevenson, W.G. (2008) The tumor microenvironment: regulation by MMP-independent effects of tissue inhibitor of metalloproteinases-2. *Cancer Metastasis Rev.*, 27, 57–66.
28. Montagna, E. *et al.* (2013) Heterogeneity of triple-negative breast cancer: histologic subtyping to inform the outcome. *Clin. Breast Cancer*, 13, 31–39.
29. Sarrió, D. *et al.* (2008) Epithelial-mesenchymal transition in breast cancer relates to the basal-like phenotype. *Cancer Res.*, 68, 989–997.
30. Cheung, K.J. *et al.* (2016) Polyclonal breast cancer metastases arise from collective dissemination of keratin 14-expressing tumor cell clusters. *Proc. Natl. Acad. Sci. U. S. A.*, 113, E854–E863.
31. Kalluri, R. *et al.* (2009) The basics of epithelial-mesenchymal transition. *J. Clin. Invest.*, 119, 1420–1428.
32. Jain, R.K. (2005) Normalization of tumor vasculature: an emerging concept in antiangiogenic therapy. *Science*, 307, 58–62.

33. Lee, S.J. *et al.* (2010) TIMP-2 modulates VEGFR-2 phosphorylation and enhances phosphodiesterase activity in endothelial cells. *Lab. Invest.*, 90, 374–382.
34. Seo, D.W. *et al.* (2011) An integrin-binding N-terminal peptide region of TIMP-2 retains potent angio-inhibitory and anti-tumorigenic activity *in vivo*. *Peptides*, 32, 1840–1848.
35. Chu, I.M. *et al.* (2008) The Cdk inhibitor p27 in human cancer: prognostic potential and relevance to anticancer therapy. *Nat. Rev. Cancer*, 8, 253–267.
36. Larrea, M.D. *et al.* (2009) p27 as Jekyll and Hyde: regulation of cell cycle and cell motility. *Cell Cycle*, 8, 3455–3461.
37. Yoon, H. *et al.* (2019) p27 transcriptionally coregulates cJun to drive programs of tumor progression. *Proc. Natl. Acad. Sci. U.S.A.*, 116, 7005–7014.
38. Wander, S.A. *et al.* (2013) PI3K/mTOR inhibition can impair tumor invasion and metastasis *in vivo* despite a lack of antiproliferative action *in vitro*: implications for targeted therapy. *Breast Cancer Res. Treat.*, 138, 369–381.
39. Malanchi, I. *et al.* (2011) Interactions between cancer stem cells and their niche govern metastatic colonization. *Nature*, 481, 85–89.
40. Bissell, M.J. *et al.* (2011) Why don't we get more cancer? A proposed role of the microenvironment in restraining cancer progression. *Nat. Med.*, 17, 320–329.
41. Jackson, H.W. *et al.* (2017) TIMPs: versatile extracellular regulators in cancer. *Nat. Rev. Cancer*, 17, 38–53.
42. Stetler-Stevenson, W.G. *et al.* (2014) Normalization of the tumor microenvironment: evidence for tissue inhibitor of metalloproteinase-2 as a cancer therapeutic. *Connect. Tissue Res.*, 55, 13–19.
43. Bourboulia, D. *et al.* (2013) TIMP-2 modulates cancer cell transcriptional profile and enhances E-cadherin/beta-catenin complex expression in A549 lung cancer cells. *Oncotarget*, 4, 166–176.
44. Kawamata, H. *et al.* (1995) Over-expression of tissue inhibitor of matrix metalloproteinases (TIMP1 and TIMP2) suppresses extravasation of pulmonary metastasis of a rat bladder carcinoma. *Int. J. Cancer*, 63, 680–687.
45. Alvarez, O.A. *et al.* (1990) Inhibition of collagenolytic activity and metastasis of tumor cells by a recombinant human tissue inhibitor of metalloproteinases. *J. Natl. Cancer Inst.*, 82, 589–595.
46. Han, H. *et al.* (2014) An endogenous inhibitor of angiogenesis inversely correlates with side population phenotype and function in human lung cancer cells. *Oncogene*, 33, 1198–1206.
47. Dey, N. *et al.* (2013) Wnt signaling in triple negative breast cancer is associated with metastasis. *BMC Cancer*, 13, 537.
48. DiMeo, T.A. *et al.* (2009) A novel lung metastasis signature links Wnt signaling with cancer cell self-renewal and epithelial-mesenchymal transition in basal-like breast cancer. *Cancer Res.*, 69, 5364–5373.
49. Yook, J.I. *et al.* (2006) A Wnt-Axin2-GSK3beta cascade regulates Snail1 activity in breast cancer cells. *Nat. Cell Biol.*, 8, 1398–1406.
50. Seo, D.W. *et al.* (2008) TIMP-2 disrupts FGF-2-induced downstream signaling pathways. *Microvasc. Res.*, 76, 145–151.
51. Oskarsson, T. *et al.* (2011) Breast cancer cells produce tenascin C as a metastatic niche component to colonize the lungs. *Nat. Med.*, 17, 867–874.